Published in final edited form as:
Photochem Photobiol. 2013 July ; 89(4): 942–952. doi:10.1111/php.12065.

PDT Dose Parameters Impact Tumoricidal Durability and Cell Death Pathways in a 3D Ovarian Cancer Model

Imran Rizvi, Ph.D.[a], **Sriram Anbil, B.S.**[a], **Nermina Alagic, M.D.**[a], **Jonathan P. Celli, Ph.D.**[a,b], **Lei Zak Zheng, Ph.D.**[a], **Akilan Palanisami, Ph.D.**[a], **Michael D. Glidden, B.S.**[a,b], **Brian W. Pogue, Ph.D.**[c], and **Tayyaba Hasan, Ph.D.**[a,*]

[a]Wellman Center for Photomedicine, Department of Dermatology, Massachusetts General Hospital, Harvard Medical School, Boston, MA, USA (IR, SA, NA, JPC, AP, MG, TH)

[b]Department of Physics, University of Massachusetts, Boston, MA 02125 (JPC, MG)

[c]Thayer School of Engineering, Dartmouth College, Hanover, NH 03755 (BWP)

Abstract

The successful implementation of photodynamic therapy (PDT)-based regimens depends on an improved understanding of the dosimetric and biological factors that govern therapeutic variability. Here, the kinetics of tumor destruction and regrowth are characterized by systematically varying benzoporphyrin derivative (BPD)-light combinations to achieve fixed PDT doses (M × J/cm^2). Three endpoints were used to evaluate treatment response: 1.) Viability evaluated every 24 hours for 5 days post-PDT; 2.) Photobleaching assessed immediately post-PDT; and 3.) Caspase-3 activation determined 24-hours post-PDT. The specific BPD-light parameters used to construct a given PDT dose significantly impact not only acute cytotoxic efficacy, but also treatment durability. For each dose, PDT with 0.25 μM BPD produces the most significant and sustained reduction in normalized viability compared to 1 μM and 10 μM BPD. Percent photobleaching correlates with normalized viability for a range of PDT doses achieved within BPD concentrations. To produce a cytotoxic response with 10 μM BPD that is comparable to 0.25 μM and 1 μM BPD a reduction in irradiance from 150 mW/cm^2 to 0.5 mW/cm^2 is required. Activated caspase-3 does not correlate with normalized viability. The parameter-dependent durability of outcomes within fixed PDT doses provides opportunities for treatment customization and improved therapeutic planning.

INTRODUCTION

Photodynamic therapy (PDT) is a light-mediated modality that involves activation of a photosensitizer (PS) to generate singlet oxygen and radical species that are toxic to cells. PDT is approved in the United States for ophthalmologic, dermatologic and oncologic applications (1–4) and is in clinical and pre-clinical evaluation for numerous cancers (3, 5–7) including intraperitoneal sarcomatoses and carcinomatoses (8–14). An array of parameters influence PDT outcomes such as PS concentration, fluence, irradiance, and the time course of cytotoxic response (15–17). These parameters provide important treatment-related challenges and opportunities that are also influenced by the therapeutic target site (3, 15–28). A disease and PS-specific characterization of outcomes that result from modulating treatment-related parameters within the framework of fixed PDT doses is necessary to

*Corresponding author: Tayyaba Hasan, PhD, thasan@mgh.harvard.edu, Phone: (617) 726-6996, Fax: (617) FAX.

SUPPLEMENTARY MATERIAL
Supplementary figures are posted online on DOI: xxxx

provide an improved understanding of potential reasons for variability in therapeutic response.

Efforts by us (18, 19, 29–38) and others (6, 16, 23, 24, 39–46) have provided insights into better predicting PDT-related outcomes through improved dosimetry and modulation of treatment protocols to account for heterogeneities in PS levels and the biological characteristics of target tissue. Zhou *et al.* (19) have reported improved treatment consistency by adjusting fluences to compensate for variations in PS concentrations to achieve a fixed PDT dose (number of photons absorbed per unit tissue). This approach resulted in more consistent changes in tumor volume compared to the group that did not receive fixed PDT doses with a clinically-approved liposomal formulation of benzoporphyrin derivative monoacid ring-A (BPD) in an orthotopic model for prostate cancer (19). However, there is significant evidence that within a PDT dose, reciprocity only holds across limited PS concentrations and is highly dependent on treatment-related parameters and the characteristics of the disease site (19, 28, 47, 48). Patterson and colleagues have recently demonstrated (24) that singlet oxygen generation, photobleaching, and cell kill efficiency decrease significantly during PDT with high intracellular concentrations of BPD. The amount of oxygen consumed per photon absorbed decreased with increasing BPD concentration and singlet oxygen dose could only be correlated with photobleaching over a limited range of BPD concentrations under aerated conditions (24). These studies were conducted with tumor cells in suspension and evaluated acute PDT efficacy with the goal of improving dosimetry and treatment customization. A clinical study by Betz *et al.* (49) assessed the therapeutic effect of m-tetrahydroxyphenylchlorin (mTHPC)-based PDT in patients with basal-cell carcinoma and showed that low PS concentrations coupled with high fluences were effective in achieving high complete response rates with the added benefit of decreased general photosensitivity. The importance of considering the biological characteristics of the target disease is highlighted in a study published by Moesta *et al.* (28), which shows different rates of photofrin photobleaching and cytotoxic efficacy between two pancreatic cancer cell-lines at a given PDT dose. In addition, a lack of reciprocity across a broad range of PS-light combinations was observed (28).

An additional critical determinant of PDT efficacy is irradiance, which has been shown by us and others to significantly impact treatment outcomes (18, 21, 25, 33, 50). Gibson *et al.* were among the first to show increased tumor destruction with lower irradiances (51). Subsequent studies by Foster and colleagues have demonstrated that consideration of irradiance is important to improving PDT efficacy (21, 52). Using 3D spheroids of EMT6/Ro mouse mammary carcinoma cells, the authors showed that irradiances of 25 and 50 mW/cm^2 provided better efficacy of Photofrin-based PDT compared to an irradiance of 200 mW/cm^2 at a fluence of 60 J/cm^2 (21). Similar results from our group and others have been reported *in vivo* with BPD-PDT (33) and aluminum pthalocyanine ($AlPcS_2$)-based PDT (25). These findings collectively highlight the need for PS and target tissue-specific characterization of outcomes that result from modulating treatment-related parameters within the framework of fixed PDT doses.

The present study evaluates the effect of systematically modulating PS-light parameters in a three-dimensional (3D) model for micrometastatic ovarian cancer (OvCa) previously established in our group (53, 54). OvCa is the fifth most common cancer among women in the United States and causes more deaths than any other gynecologic malignancy (55–57). Despite significant advancements in surgical techniques and improvements in the medical management of advanced stage OvCa, survival rates remain dismal (55–57). There is a need to identify new mechanistically distinct therapeutic strategies that complement conventional treatments to improve outcomes from this lethal disease.

PDT is mechanistically-distinct from conventional therapies and is being evaluated for the treatment of an array of solid tumors including malignant intracranial cancers (58–63), head and neck cancers (64–66), recurrent prostate adenocarcinoma (67), bladder cancer (68), cholangiocarcinoma (69), pancreatic and bile duct cancers (70–73), as well as a variety of intraperitoneal carcinomatoses and sarcomatoses, including disseminated OvCa (8–14). Depending on the choice and concentration of PS, and other treatment-related parameters, a range of cell death pathways can be triggered by PDT including necrosis, apoptosis and autophagy (74–79). The mechanisms that trigger the various death pathways and molecular responses to PDT are complex and beyond the scope of this article. We refer the reader to a few, among many, elegant reviews and articles on this topic (3, 15, 17, 26, 74–77, 79–84). For BPD, the mitochondrion is a preferential, but not exclusive, site of sub-cellular localization (85–92). Light-mediated activation of BPD, can cause photodamage to the anti-apoptotic protein bcl-2 as well as the mitochondrion (20, 79, 86, 88, 93, 94). Depending on the PS concentration, target cells, PDT dose, and other biological and therapeutic variables, this photodamage triggers a rapid release of cytochrome c and the activation of a cascade of caspases (75, 86–88, 90–92). These caspases, such as the “effector” or “executioner” caspase 3, catalyze the hydrolytic reactions of apoptosis (75, 86–88, 90–92). This example of the potency and mechanistic breadth by which BPD-PDT confers cytotoxicity is illustrative of the factors that make PDT an important therapeutic tool in the development of rationally-designed treatment strategies for many diseases including metastatic OvCa. Leveraging these mechanistic assets, preclinical studies have shown that PDT reverses chemoresistance, synergistically enhances the efficacy of traditional chemotherapeutics and biologics, and reduces chemotherapy cycles (54, 95, 96). PDT disrupts and reduces the size of 3D ovarian micronodules, which addresses some of the key barriers to improved treatment efficacy in OvCa (53, 54). With these promising insights, it remains unclear which PDT parameters (e.g. PDT dose, PS-light combinations, and irradiances) will provide the most significant and sustained cytotoxic response in the treatment of multifocal tumors. An array of research tools and perspectives will be required to address the complexities of therapeutic variability.

Building on the elegant work of others to improve the predictability of PDT outcomes (6, 7, 15, 16, 24, 28, 75, 79, 97–102) as well as efforts by us (18, 19, 29, 30, 103), here the effects of modulating dose-related parameters on the extent and durability of PDT efficacy is assessed. A 3D model that restores important biological and architectural cues for adherent micrometastatic OvCa is used (Figure 1, left) (53, 54). A matrix of PS-light combinations that constitute three fixed PDT doses (Figure 1, middle) provides the framework to evaluate a few key determinants of cytotoxic response (Figure 1, right) among the many factors that warrant investigation. The effect of modulating PDT parameters is evaluated by administering BPD concentrations of 0.25 μM, 1 μM, or 10 μM (Figure 1, middle, blue) and appropriate fluences (0.125 J/cm^2 – 40 J/cm^2 at 150 mW/cm^2) (Figure 1, middle, red) to achieve three fixed PDT doses (1.25, 5, or 10 μM × J/cm^2) (Figure 1, middle, purple). Cytotoxic efficacy is evaluated every 24 hours for 5 days post-PDT using viability as a metric for therapeutic efficacy (Figure 1, right). Photobleaching is assessed immediately post-PDT as a surrogate measurement of the photodynamic events that produce concentration-dependent cytotoxic outcomes within fixed PDT doses. The impact of modulating irradiance on PDT efficacy is evaluated using viability 24 hours post-PDT as a cytotoxic endpoint. Additionally, activation of caspase-3 as a late stage apoptosis marker, is assessed 24 hours post-PDT.

MATERIALS AND METHODS

Cell Lines

Human ovarian carcinoma cells NIH:OVCAR5 (OVCAR5) were obtained from Fox Chase Cancer Center (Philadelphia, PA, USA), where they were characterized by microsatellite marker analysis. The cells were grown in RPMI 1640 (Roswell Park Memorial Institute) medium (Mediatech Inc., Herndon, Virginia, USA) and supplemented with 10% heat inactivated fetal calf serum (GIBCO Life Technologies, Grand Island, New York, USA), 100 U/mL penicillin, and 100 μg/mL streptomycin. Growth factor reduced (GFR) Matrigel (Catalog number 354230, BD Biosciences, San Jose, California, USA) was used as a basement membrane in 3D cultures.

3D ovarian cancer model

GFR Matrigel beds were prepared by pipetting 250 μL of GFR Matrigel solution at −4 °C on chilled 24-well plates. The plates were incubated for 30 minutes at 37 °C to allow for gelation. OVCAR5 cells were plated on the prepared beds on ice in black-walled 24-well plates at a density of 7500 cells in 1 mL of 2% GFR Matrigel medium. The 3D Ovarian cultures were then incubated at 37°C in an atmosphere of 5% CO2 for 10 days. The 3D culture was maintained with a 2% GFR-Matrigel RPMI 1640 solution and was changed every 3 to 4 days.

Photodynamic therapy

Ten days following plating, cultures were incubated with 0.25 μM, 1 μM and 10 μM BPD (QLT, Inc., Vancouver, British Columbia, Canada) in complete culture media for 90 min. The media were replaced with 2% GFR-Matrigel medium immediately prior to irradiation. Each well was irradiated with a 690-nm fiber-coupled diode laser (Model 7401; High Power Devices, Inc., North Brunswick, NJ, USA) using irradiances ranging from of 0.5–150 mW/cm^2, which were measured using an Ophir Vega power meter with photodiode sensor (Ophir Optronics, Israel) prior to each experiment. Three-dimensional nodules were treated with total PDT doses ([PS] × fluence) of 1.25, 5, and 10 μM × J/cm^2 at each BPD concentration (0.25 μM, 1 μM and 10 μM). Irradiation times were calculated automatically by using custom-written IGOR scripts (Wavemetrics, Lake Oswego, OR, USA) and laser irradiations were controlled by a custom-built shutter system.

Photobleaching

Photobleaching was evaluated in 10 day old 3D ovarian cancer nodules incubated with 0.25 μM, 1 μM, or 10 μM BPD for 90 minutes in complete growth media. Briefly, images of BPD fluorescence were acquired pre and immediately post-PDT using previously established settings (104). Percent photobleaching was estimated from the following formula as previously described (104):

$$\%\ \text{Photobleaching} = -\left(\frac{\text{Post PDT Fluorescence Intensity} - \text{Pre PDT Fluorescence Intensity}}{\text{Pre PDT Fluorescence Intensity}}\right) \times 100$$

Cryosectioning of 3D cultures

OVCAR5 3D micronodules were sectioned using an HM 550 cryostat (Richard-Allen Scientific) as previously described (105). Samples were sectioned to a thickness of 35 μm and stained with DAPI (Sigma) to visualize cell nuclei. Images were acquired 24 hours after sectioning with the Olympus FV-1000 confocal microscope at an objective magnification of 40x (NA=0.75).

Quantification of cytotoxic response in 3D cultures

Cytotoxic response to PDT treatments on 3D cultures was assessed by an imaging-based methodology as previously described (106, 107). Briefly, cultures were stained, in situ, with calcein AM and ethidium bromide (to label live and dead cells respectively) prior to imaging using an Olympus FV-1000 confocal microscope. Images were batch-processed in MATLAB using a custom routine to segment the fluorescence channels and determine pixel intensities for the Calcein (live) and Ethidium bromide (dead) channels separately averaged within individual nodules or across the entire field of view. Subsequently, individual nodule viabilities and overall nodule viability for the viewing field was calculated from the mean intensities as reported by the normalized, and appropriately scaled ratio of fluorescent signals (calcein divided the sum of calcein plus ethidium bromide) as extensively described in previous publications (53, 54, 108–110).

ELISA for activated Caspase-3

Twenty-four hours following PDT treatment, 3D cultures in 24-well plate were carefully washed 3 times with PBS and then 1 ml of MatriSperse Cell Recovery Solution (BD Biosciences) was added into each well and incubated on ice for 30 min to dissolve the Matrigel bed and gently release the tumor acini. Detached tumor acini were collected and washed twice in 1 ml of fresh cold MatriSperse to remove the residue Matrigel. Pelleted acini were dissolved with protein extraction buffer provided in the ELISA kit for cleaved caspase-3 (Cell Signaling) by following the manufacturer's suggested protocol. Ten μl of the soluble protein fraction were used for ELISA measurement of cleaved caspase-3, and the results were normalized to the total protein concentration of each sample, and plotted as fold-increase relative to no treatment controls. Values represent averages of duplicates for each group from 2 platings.

Statistical Analysis

Comparisons of cytotoxic efficacy and BPD fluorescence were performed by one-way ANOVA or two-tailed t-test, as appropriate. Unlabeled comparisons indicate a two-tailed t-test. Linear regressions were evaluated by a least squares fit approach and correlation coefficients were determined using Pearson's product-moment correlation method. Error bars indicate s.e.m. A P value of less than 0.05 was considered significant.

RESULTS

For a given PDT dose, 0.25 μM BPD-PDT results in the most significant and sustained reduction in normalized viability

To assess the impact on cytotoxic response of modulating PS-light parameters within fixed PDT doses, OVCAR5 3D nodules were incubated with either 0.25 μM BPD (blue), 1 μM BPD (red), or 10 μM BPD (green) and treated with appropriate fluences to achieve three PDT doses: 1.25, 5, and 10 μM × J/cm^2 (Figure 1). Relative to no treatment (black), the most significant and most sustained reduction in normalized viability was seen in nodules treated with 0.25 μM BPD-PDT compared to 1 μM and 10 μM BPD-PDT for all PDT doses (one-way ANOVA) (Figure 2A). The lowest viabilities over all PDT doses and all concentrations were observed 72 hours (0.09 ± 0.01) and 96 hours (0.10 ± 0.01) post-PDT in nodules treated with 0.25 μM BPD-PDT at a dose of 10 μm × J/cm^2 ($p<0.05$; one-way ANOVA). These viabilities at 72 and 96 hours were not significantly different from each other. At a dose of 5 μm × J/cm^2, viabilities of nodules treated with 0.25 μM BPD-PDT were significantly lower (0.16 ± 0.02 and 0.19 ± 0.02, respectively) than those treated with 1 μM BPD-PDT (0.30 ± 0.01 and 0.45 ± 0.04, respectively). At a PDT dose of 1.25 μm × J/cm^2, normalized viabilities of nodules treated with 0.25 μM or 1 μM BPD-PDT were not

significantly different for the first 72 hours post-PDT. Nodules treated with 10 μM BPD-PDT consistently showed the poorest response, with normalized viabilities that were significantly greater than 0.25 and 1 μM BPD-PDT for all doses across all time points (one-way ANOVA).

Figure 2B shows representative LIVE/DEAD images of OvCa 3D micronodules that were used to generate the values for normalized viability in Figure 2A. Images depict nodules evaluated 72 hours following PDT using different PS-light parameters to achieve a fixed dose of 10 μM × J/cm^2. Relative to no treatment controls (1), increased killing is observed in nodules treated with 0.25 μM BPD-PDT (4) compared to either 1 μM BPD-PDT (3) or 10 μM BPD-PDT (2), as evidenced by increased ethidium bromide fluorescence (red) and decreased calcein fluorescence (green).

Normalized viability correlates linearly with percent photobleaching within BPD concentrations

Photobleaching was measured in nodules treated using 0.25 μM (blue), 1 μM (red) or 10 μM (green) BPD at PDT doses of 1.25 μM × J/cm^2 (circled), and 5 and 10 μM × J/cm^2 (second and third points, respectively, on each correlation line within a concentration). Percent photobleaching (evaluated immediately post-PDT) correlates with normalized viabilities across PDT doses (assessed 24 hours post-PDT), within each BPD concentration (Figure 3). The goodness of fit values (r^2) for linear regressions within each BPD concentration were 0.9962 for 0.25 μM BPD (blue), 0.9332 for 1 μM BPD (red), and 0.9982 for 10 μM BPD (green) (error bars indicate s.e.m. N ≥4 wells for each data point). The p value for all correlations was less than 0.05. Representative unadjusted images of BPD fluorescence used to generate Figure 3 are shown in Supplemental Figure 1.

BPD fluorescence from 3D ovarian micronodule sections indicates penetration throughout 3D micronodules and a concentration-dependent BPD uptake

To evaluate concentration-dependent BPD distribution and uptake in 3D micronodules, 10 day old cultures were incubated with 0.25 μM, 1 μM and 10 μM BPD for 90 minutes, then cryosectioned, and imaged (Figure 4). (A) Representative fluorescence images of BPD (red) and DAPI (blue) along with corresponding BPD fluorescence intensity profiles (B) show that BPD is distributed throughout tumor micronodules at all concentrations: 0.25 μM (blue), 1 μM (red), and 10 μM (green). (C) BPD fluorescence intensity increased in a concentration-dependent manner. Mean fluorescence intensity was significantly lower at a concentration of 0.25 μM ($2.07 \times 10^5 \pm 7.04 \times 10^4$)(blue), compared to 1 μM ($1.23 \times 10^6 \pm 2.06 \times 10^5$)(red) and 10 μM BPD ($1.46 \times 10^7 \pm 2.50 \times 10^6$) (green) ($p$<0.05, one-way ANOVA, n=5 for each concentration, error bars indicate s.e.m.). As shown in representative images in Supplemental Figure 2, BPD fluorescence was evenly distributed throughout the 3D nodules following PDT, irrespective of the PS concentration. Mean BPD fluorescence intensities varied significantly post-PDT (n=4 nodules for 0.25 μM BPD and n=6 for 10 μM BPD).

Decreasing irradiance improves PDT efficacy in 3D OvCa nodules

Informed by previously published findings (18, 21, 25, 33, 50), the impact of modulating irradiance on PDT efficacy was assessed in 3D OvCa nodules (Figure 5). A fixed PDT dose of 1.25 μM × J/cm^2 was administered using 10 μM BPD (green) and irradiances ranging from 150 mW/cm^2 to 0.5 mW/cm^2. Normalized viability was significantly higher at an irradiance of 150 mW/cm^2 (0.93 ± 0.01) than all lower irradiances (p<0.05, one-way ANOVA, N=6). An irradiance of 0.5 mW/cm^2 was necessary to achieve a reduction in normalized viability with 10 μM BPD-PDT (0.69 ± 0.02) to levels that were not significantly different from 0.25 μM (0.63 ± 0.03)(blue) and 1 μM BPD-PDT (0.73 ± 0.03)

(red). This reduction in normalized viability at the lower irradiance required a substantial increase in the irradiation time from approximately 1 second at 150 mW/cm^2 to 250 seconds at 0.5 mW/cm^2. An asymptotic exponential growth model was used to fit viability and irradiance for nodules treated with 10 μM BPD-PDT (r^2=0.8411).

Activated caspase-3 correlates with PDT dose under limited conditions

There was no relationship between activated caspase-3 levels and PDT dose for concentrations of 0.25 μM (blue) and 1 μM BPD (red) (Figure 6). A monotonic increase in caspase-3 activation was observed with increasing PDT dose using 10 μM BPD (green) (r^2 = 0.995, P<0.05). Relative to no treatment controls, activated caspase-3 levels increased in all PDT treated groups. The most significant increase in activated caspase-3 levels was observed in the group treated with a PDT dose of 10 μM × J/cm^2 BPD-PDT using 10 μM BPD (mean fold increase = 22.5 ± 2.0) (P<0.05, one-way ANOVA). Among the group treated with a PDT dose of 5 μM × J/cm^2, the most significant increase in activated caspase-3 was seen in nodules treated with 1 μM BPD (mean fold increase = 20.7 ±1.3) (P<0.05, one-way ANOVA). For the groups treated with the lowest PDT dose, both 0.25 μM and 1 μM BPD induced the highest increases in activated caspase-3 (mean fold increase = 7.0 ±0.18 and 7.8 ±0.37, respectively) compared to 10 μM BPD (mean fold increase = 4.1±0.43).

DISCUSSION

Pre-clinical (54, 96, 111–118) and clinical (9–12, 119, 120) evidence suggests that PDT is a promising modality for the treatment of intraperitoneal malignancies, including disseminated OvCa. Due to the diverse biology of advanced stage disease and the narrow therapeutic index associated with treating complex sites such as the peritoneal cavity, PDT will most likely be part of a rationally-designed, multifaceted treatment plan (15, 81, 82, 118, 119). As with any treatment, the successful implementation of PDT-based regimens depends in part on improved dosimetric tools (6, 19, 24, 29, 39, 41, 97, 99, 112, 121, 122) along with a better understanding of the biological characteristics of the target tissue that govern optimal therapeutic response (28, 74, 75, 79, 101, 123, 124). Here, a systematic analysis of the tumoricidal effects that result from modulating PDT parameters is conducted to longitudinally characterize outcomes that may be relevant to developing comprehensive treatment strategies in the management of multifocal OvCa (53, 54, 125–129). The present study focuses on the following therapeutic and biological parameters among the many that warrant consideration: (i) the time-dependent evolution of cytotoxicity and regrowth resulting from systematically varying PS-light combinations to construct fixed PDT doses; (ii) the correlation between viability and photobleaching as a potentially relevant tool for implicit dosimetry; (iii) the effect of modulating irradiance on tumor viability; and (iv) the relationship between cytotoxicity and the activation of a marker for apoptotic cell death, caspase-3. Our findings demonstrate that the kinetics of tumor destruction and regrowth are significantly impacted by the parameters used to construct a given PDT dose. This study builds on efforts by us (18, 19, 29–38) and others (6, 16, 23, 24, 39–46) to improve the predictability of PDT outcomes through a better understanding of the biological and dosimetric factors that contribute to variability in treatment response.

PDT dosimetry is a complex and active area of study that can be approached from several perspectives, including implicit and explicit measurement of treatment-related variables, as described by Wilson and colleagues (24, 97, 122). Explicit dosimetry requires direct measurement of multiple independent photodynamic parameters that influence efficacy, such as local PS concentration, delivered light dose, and reactive oxygen species (24, 97). However, obtaining real-time measurements of each, or a combination of these parameters can be cumbersome, and reliable techniques and instrumentation are being investigated (40,

42, 130, 131). Implicit dosimetry may be a more feasible approach because it involves quantification of more readily accessible dosimetric parameters, such as PS photobleaching, which may be indicative of the photodynamic events that determine therapeutic efficacy (24, 97, 112, 121, 122). A study published by Ascencio *et al.* demonstrates that protoporphyrin IX photobleaching correlates strongly (r^2=0.89) with necrotic score after intraperitoneal hexaminolevulinate (HAL)-based PDT of OvCa in rats (112). Dysart *et al.* have shown that photobleaching following mTHPC-based PDT can predict the viability of murine erythroleukemic cells in suspension (at PS concentrations below 2 μg/ml) (121). Weston *et al.* demonstrated that an implicit photobleaching-based metric correlates well with the viability of rat prostate adenocarcinoma cells in suspension after BPD-PDT (24). This correlation was true under oxygenated conditions for BPD concentrations of approximately 0.1 μM, 0.7 μM, and 3.5 μM (24). The study by Weston *et al.*(24) and the present study could only establish a correlation between cytotoxic efficacy and BPD photobleaching within limited ranges of BPD concentrations. Within the limited dose ranges evaluated in the present study (Figure 3), the rate of change in viability relative to percent photobleaching may be highest for 10 μM BPD-PDT compared to 0.25 and 1 μM BPD-PDT. The slopes for these correlations were not significantly different across BPD concentrations in this small, discrete dataset. It is worth noting that for 10 μM BPD-PDT the total change in viability and percent photobleaching occurred over a limited range, and additional studies are necessary to evaluate the scope of these relationships. These results are supported by the observation that photobleaching correlates with singlet oxygen production for limited ranges of BPD concentrations when the availability of local oxygen is not rate limiting (24).

Additional factors that may account for the concentration-dependent variability in therapeutic outcomes observed in the present study include PS aggregation, altered subcellular localization, differential photochemical mechanisms, microenvironmental influences, and self-shielding by the PS (20, 38, 44, 45, 100, 132, 133). Elegant studies by Aveline et al.(20, 38, 46, 134) have shown that the biological microenvironment can significantly impact PS photophysics and photochemistry. Local concentrations of PS and oxygen influence the photosensitizaion mechanisms of porphyrins in a cell. A reduction in the fluorescence and triplet state quantum yields is observed with increasing concentrations of many porphyrin PS, including BPD (38, 134). Foster and colleagues have demonstrated differential mechanisms of PS photobleaching that impact photodynamic dosimetry (44, 45, 135). Self-shielding is observed when sufficiently high PS concentrations prevent uniform light absorption (100). As shown in Supplemental Figure 2, BPD appears to be uniformly distributed across multiple cell layers following PDT treatment of 3D OvCa nodules at a dose of 5 μM × J/cm^2 using either 0.25 μM (n=4) or 10 μM (n=6) BPD. These results from representative cryosectioned tumors per BPD concentration suggest that self-shielding at the size range evaluated here (~ 150 μm in diameter) may play only a small role in explaining the observed parameter-dependent discrepancies in cytotoxicity and photobleaching. Additional studies are necessary to characterize the potential role of concentration-dependent shielding that may be occurring at the subcellular level as well as in tumors that are outside the size range evaluated here.

In addition to these and other dosimetric approaches that may improve the predictability of treatment outcomes, an understanding of the molecular mechanisms that lead to cell death will be important considerations in PDT-related treatment planning. Caspase-3 is an executioner caspase that is activated by many death pathways and is thought to be a critical player in the events that lead to apoptosis (75, 101, 136). Oleinick and colleagues have shown differential kinetics and pathways for PDT-based destruction of breast cancer cells, dependent in part on the procaspase-3 status of the cells (101, 136). An increase in PDT-induced DNA fragmentation, among other hallmarks of apoptosis, were observed with increased expression of activated caspase-3 (136). Depending on the procaspase-3 status,

there was also a differential sensitivity to PDT as evaluated by the WST-1 assay, which measures the ability of mitochondria to reduce a tetrazolium dye (136). However, the critical lethal events that compromise the ability of cells to divide and form colonies and ultimately lead to tumor destruction were independent of caspase-3 activation, both in monolayer and *in vivo* (75, 101, 136). These findings highlight the importance of understanding the metrics used to evaluate cytotoxic response within the context of the biological and microenviromental characteristics of the target tissue. The present study in a 3D OvCa model supports these findings, where no correlation was observed between caspase-3 activation and PDT dose (Figure 6) with 0.25 μM and 1 μM BPD-PDT. There was a correlation between PDT dose and caspase-3 activation with 10 μM BPD-PDT (Figure 6). Any potential relationship between caspase-3 activation and cytotoxicity seemed to be limited to low levels of cell killing with 10 μM BPD-PDT (Figure 2 and Figure 6). The nature and significance of this trend remains unclear and suggests a system-dependent activation of complex cell death pathways and survival processes that have been described previously (76, 90, 101, 136–138), and need to be explored further.

An understanding of the molecular characteristics of the target tissue may be important to determining the broader implications of the differential responses to PDT observed in a 3D tumor model using one tumor cell line. In contrast to the findings from the present study, Kessel and colleagues have shown that PDT with 10 μM BPD is significantly more effective than 1 μM BPD at reducing colony formation in a murine hepatoma cell line across a range of equivalent PDT doses (79). The authors suggest that in instances where autophagy serves as a protective mechanism against phototoxicity, the use of high concentrations of BPD could potentiate PDT efficacy (79). The basis for this idea is informed in part by a study from Donohue (139) *et al.* showing that BPD interferes with the sequestration and degradation of cytoplasmic material and inhibits the formation of autophagosomes in a concentration dependent manner. Osaki *et al.* have shown that BPD-PDT is differentially effective in four different types of rodent cell lines, due in part to variability in uptake and intracellular localization of the photosensitizer (140). A study by Moesta *et al.* (28) supports the importance of evaluating the effects of modulating PDT dose parameters in a manner that accounts for differences in the biological characteristics of the target tissue. Even within a given disease, variability between cell lines influences uptake and localization of the PS as well as the photophysical and photochemical events that determine overall response to treatment (28).

PDT has been shown to enhance the efficacy of traditional chemo- and biological-therapies, and should be included as part of rationally-designed combination treatment regimens (54, 95, 96, 141). Among the many factors that govern the successful development of PDT-based combinations, an understanding of the optimal dose and scheduling for the individual monotherapies based, in part, on the extent and durability of the cytotoxic response is required. A previous study from our laboratory has shown that PDT synergistically enhances carboplatin efficacy in a sequence-dependent manner (54). The synergistic regimen involved administration of carboplatin immediately after treatment with a PDT dose of 1.25 μM × J/cm^2 delivered using 0.25 μM BPD and 5J/cm^2 (54). The present study indicates that these same parameters confer the most significant reduction in the normalized viability, but the tumoricidal response continues to evolve for several days following treatment. It remains unclear whether the application of chemotherapy agents immediately after PDT or at the peak of PDT-induced cytotoxicity would maximize the cooperative interaction between the treatments. Additionally, weighing treatment-associated toxicity against increased efficacy *in vivo* will be an important consideration when determining the appropriate PDT dose-related parameters (142).

CONCLUSIONS

In the past few years, there has been an increasing focus towards the customization of targeted therapies informed by patient-specific molecular profiles of the target disease (143). Similarly, cytotoxic modalities such as PDT could benefit from therapeutic planning based on the identification of key molecular signatures that will guide the customization of treatment-related parameters. The present study demonstrates that using low concentrations of BPD and correspondingly high fluences to construct a PDT dose provides maximal tumoricidal efficacy and durability. It is important to note that while these results were assessed in a 3D OvCa model, other studies have identified differential PDT parameters that were optimal in other systems (22, 28, 79, 144). Percent photobleaching correlates with a reduction in normalized viability only within given BPD concentrations used to achieve a range of fixed PDT doses. These findings, supported by others (24, 97, 112, 121, 122), suggest that implicit dosimetry is a complex technique that must be informed in part by the specific parameters used to construct a given PDT dose. Building on the elegant work of others and efforts by us (18, 21, 25, 33, 50), the present study shows that low irradiance improves treatment efficacy for a PS-light combination that otherwise results in poor response. A correlation between PDT dose and activated caspase-3 was only observed with high BPD concentrations, where minimal killing was evident. Activated caspase-3 did not correlate with normalized viability across all BPD concentrations and time points evaluated, highlighting the complexity of death pathways that has been supported by other groups (76, 90, 101, 136–138). Collectively, these findings suggest that PDT delivery parameters could be customized based in part on a better understanding of the molecular signatures and biological characteristics of target sites.

Supplementary Material

Refer to Web version on PubMed Central for supplementary material.

Acknowledgments

Dr. Hasan and Dr. Celli wish to acknowledge support from the following grants from the National Cancer Institute at the National Institutes of Health: R01CA158415, R01CA160998 (TH) and K99CA155045 (JPC). Dr. Celli also acknowledges support from the Eleanor and Miles Shore Fellowship Program for Scholars in Medicine.

References

1. Huang Z. A review of progress in clinical photodynamic therapy. Technol Cancer Res Treat. 2005; 4:283–93. [PubMed: 15896084]
2. NCI. Photodynamic Therapy for Cancer. 2010. Available at: http://www.cancer.gov/cancertopics/factsheet/Therapy/photodynamic
3. Hasan, T.; Ortel, B.; Solban, N.; Pogue, B. Photodynamic therapy of cancer. In: Kufe, DW.; Bast, RCJ.; Hait, WN.; Hong, WK.; Pollock, RE.; Weichselbaum, RR.; Holland, JF.; Frei, EI., editors. Cancer Medicine. B.C. Decker, Inc; Hamilton, Ontario: 2006. p. 537-48.
4. Smits T, Moor AC. New aspects in photodynamic therapy of actinic keratoses. J Photochem Photobiol B. 2009; 96:159–69. [PubMed: 19592269]
5. Brown S, Brown E, Walker I. The present and future role of photodynamic therapy in cancer treatment. Lancet Oncology. 2004; 5:497–508. [PubMed: 15288239]
6. Wilson B, Patterson M. The physics, biophysics and technology of photodynamic therapy. Phys Med Biol. 2008; 53:61. [PubMed: 18182687]
7. Wilson BC. Photodynamic therapy for cancer: principles. Can J Gastroenterol. 2002; 16:393–6. [PubMed: 12096303]
8. Busch TM, Hahn SM, Wileyto EP, Koch CJ, Fraker DL, Zhang P, Putt M, Gleason K, Shin DB, Emanuele MJ, Jenkins K, Glatstein E, Evans SM. Hypoxia and Photofrin uptake in the

intraperitoneal carcinomatosis and sarcomatosis of photodynamic therapy patients. Clin Cancer Res. 2004; 10:4630–8. [PubMed: 15269134]

9. Hahn SM, Fraker DL, Mick R, Metz J, Busch TM, Smith D, Zhu T, Rodriguez C, Dimofte A, Spitz F. A Phase II Trial of Intraperitoneal Photodynamic Therapy for Patients with Peritoneal Carcinomatosis and Sarcomatosis. Clinical Cancer Research. 2006; 12:2517. [PubMed: 16638861]
10. DeLaney TF, Sindelar WF, Tochner Z, Smith PD, Friauf WS, Thomas G, Dachowski L, Cole JW, Steinberg SM, Glatstein E. Phase I study of debulking surgery and photodynamic therapy for disseminated intraperitoneal tumors. International journal of radiation oncology, biology, physics. 1993; 25:445–57.
11. Sindelar WF, DeLaney TF, Tochner Z, Thomas GF, Dachoswki LJ, Smith PD, Friauf WS, Cole JW, Glatstein E. Technique of photodynamic therapy for disseminated intraperitoneal malignant neoplasms. Phase I study. Arch Surg. 1991; 126:318–24. [PubMed: 1998474]
12. Hendren SK, Hahn SM, Spitz FR, Bauer TW, Rubin SC, Zhu T, Glatstein E, Fraker DL. Phase II trial of debulking surgery and photodynamic therapy for disseminated intraperitoneal tumors. Annals of Surgical Oncology. 2001; 8:65–71. [PubMed: 11206227]
13. Wilson JJ, Jones H, Burock M, Smith D, Fraker DL, Metz J, Glatstein E, Hahn SM. Patterns of recurrence in patients treated with photodynamic therapy for intraperitoneal carcinomatosis and sarcomatosis. Int J Oncol. 2004; 24:711–7. [PubMed: 14767557]
14. Wierrani F, Fiedler D, Grin W, Henry M, Dienes E, Gharehbaghi K, Krammer B, Grunberger W. Clinical effect of meso-tetrahydroxyphenylchlorine based photodynamic therapy in recurrent carcinoma of the ovary: preliminary results. Br J Obstet Gynaecol. 1997; 104:376–8. [PubMed: 9091020]
15. Agostinis P, Berg K, Cengel KA, Foster TH, Girotti AW, Gollnick SO, Hahn SM, Hamblin MR, Juzeniene A, Kessel D, Korbelik M, Moan J, Mroz P, Nowis D, Piette J, Wilson BC, Golab J. Photodynamic therapy of cancer: an update. CA Cancer J Clin. 2011; 61:250–81. [PubMed: 21617154]
16. Jarvi M, Patterson M, Wilson B. Insights into photodynamic therapy dosimetry: simultaneous singlet oxygen luminescence and photosensitizer photobleaching measurements. Biophysical journal. 2012; 102:661–732. [PubMed: 22325290]
17. Celli JP, Spring BQ, Rizvi I, Evans CL, Samkoe KS, Verma S, Pogue BW, Hasan T. Imaging and photodynamic therapy: mechanisms, monitoring, and optimization. Chem Rev. 2010; 110:2795–838. [PubMed: 20353192]
18. Pogue BW, Hasan T. A theoretical study of light fractionation and dose-rate effects in photodynamic therapy. Radiat Res. 1997; 147:551–9. [PubMed: 9146700]
19. Zhou X, Pogue BW, Chen B, Demidenko E, Joshi R, Hoopes J, Hasan T. Pretreatment photosensitizer dosimetry reduces variation in tumor response. Int J Radiat Oncol Biol Phys. 2006; 64:1211–20. [PubMed: 16504761]
20. Aveline B, Hasan T, Redmond RW. Photophysical and photosensitizing properties of benzoporphyrin derivative monoacid ring A (BPD-MA). Photochemistry and photobiology. 1994; 59:328–35. [PubMed: 8016212]
21. Foster TH, Hartley DF, Nichols MG, Hilf R. Fluence rate effects in photodynamic therapy of multicell tumor spheroids. Cancer Res. 1993; 53:1249–54. [PubMed: 8443805]
22. Gibson SL, Havens JJ, Foster TH, Hilf R. Time-dependent intracellular accumulation of delta-aminolevulinic acid, induction of porphyrin synthesis and subsequent phototoxity. Photochem Photobiol. 1997; 65:416–421. [PubMed: 9077122]
23. Finlay JC, Mitra S, Patterson MS, Foster TH. Photobleaching kinetics of Photofrin in vivo and in multicell tumour spheroids indicate two simultaneous bleaching mechanisms. Phys Med Biol. 2004; 49:4837–60. [PubMed: 15584523]
24. Weston M, Patterson M. Calculation of singlet oxygen dose using explicit and implicit dose metrics during benzoporphyrin derivative monoacid ring A (BPD-MA)-PDT in vitro and correlation with MLL cell survival. Photochemistry and photobiology. 2011; 87:1129–1166. [PubMed: 21575000]
25. Henderson B, Busch T, Snyder J. Fluence rate as a modulator of PDT mechanisms. Lasers in surgery and medicine. 2006; 38:489–582. [PubMed: 16615136]

26. Dougherty TJ, Gomer CJ, Henderson BW, Jori G, Kessel D, Korbelik M, Moan J, Peng Q. Photodynamic therapy. Journal of the National Cancer Institute. 1998; 90:889–905. [PubMed: 9637138]
27. Hopper C. Photodynamic therapy: a clinical reality in the treatment of cancer. Lancet Oncol. 2000; 1:212–9. [PubMed: 11905638]
28. Moesta KT, Greco WR, Nurse-Finlay SO, Parsons JC, Mang TS. Lack of reciprocity in drug and light dose dependence of photodynamic therapy of pancreatic adenocarcinoma in vitro. Cancer research. 1995; 55:3078–84. [PubMed: 7606730]
29. Lilge L, Molpus K, Hasan T, Wilson BC. Light dosimetry for intraperitoneal photodynamic therapy in a murine xenograft model of human epithelial ovarian carcinoma. Photochem Photobiol. 1998; 68:281–8. [PubMed: 9747583]
30. Lee S, Galbally-Kinney K, Hinds M, O'Hara J, Pogue B, Liang A, Hasan T, Davis S. A singlet oxygen monitor as an in vivo photodynamic therapy dosimeter. SPIE Proceedings from Photodynamic Therapy: Back to the Future. 2009; 7380:738046.
31. Pogue BW, Sheng C, Benevides J, Forcione D, Puricelli B, Nishioka N, Hasan T. Protoporphyrin IX fluorescence photobleaching increases with the use of fractionated irradiation in the esophagus. Journal of Biomedical Optics. 2008; 13:10.
32. Samkoe KS, Chen A, Rizvi I, O'Hara JA, Hoopes PJ, Pereira SP, Hasan T, Pogue BW. Imaging tumor variation in response to photodynamic therapy in pancreatic cancer xenograft models. Int J Radiat Oncol Biol Phys. 2010; 76:251–9. [PubMed: 20005458]
33. Iinuma S, Schomacker KT, Wagnieres G, Rajadhyaksha M, Bamberg M, Momma T, Hasan T. In vivo fluence rate and fractionation effects on tumor response and photobleaching: photodynamic therapy with two photosensitizers in an orthotopic rat tumor model. Cancer Res. 1999; 59:6164–70. [PubMed: 10626808]
34. Laubach H, Chang S, Lee S, Rizvi I, Zurakowski D, Davis S, Taylor C, Hasan T. In-vivo singlet oxygen dosimetry of clinical 5-aminolevulinic acid photodynamic therapy. Journal of Biomedical Optics. 2008; 13:050504. [PubMed: 19021376]
35. Ortel B, Chen N, Brissette J, Dotto GP, Maytin E, Hasan T. Differentiation-specific increase in ALA-induced protoporphyrin IX accumulation in primary mouse keratinocytes. Br J Cancer. 1998; 77:1744–51. [PubMed: 9667642]
36. Ortel B, Sharlin D, O'Donnell D, Sinha AK, Maytin EV, Hasan T. Differentiation enhances aminolevulinic acid-dependent photodynamic treatment of LNCaP prostate cancer cells. Br J Cancer. 2002; 87:1321–7. [PubMed: 12439724]
37. Chang SK, Rizvi I, Solban N, Hasan T. In vivo optical molecular imaging of vascular endothelial growth factor for monitoring cancer treatment. Clin Cancer Res. 2008; 14:4146–53. [PubMed: 18593993]
38. Aveline BM, Hasan T, Redmond RW. The effects of aggregation, protein binding and cellular incorporation on the photophysical properties of benzoporphyrin derivative monoacid ring A (BPDMA). Journal of photochemistry and photobiology B, Biology. 1995; 30:161–9.
39. Dysart JS, Patterson MS. Photobleaching kinetics, photoproduct formation, and dose estimation during ALA induced PpIX PDT of MLL cells under well oxygenated and hypoxic conditions. Photochemical & photobiological sciences: Official journal of the European Photochemistry Association and the European Society for Photobiology. 2006; 5:73–81.
40. Jarvi M, Niedre M, Patterson M, Wilson B. Singlet oxygen luminescence dosimetry (SOLD) for photodynamic therapy: current status, challenges and future prospects. Photochemistry and photobiology. 2006; 82:1198–1210. [PubMed: 16808593]
41. Dysart JS, Patterson MS. Characterization of Photofrin photobleaching for singlet oxygen dose estimation during photodynamic therapy of MLL cells in vitro. Phys Med Biol. 2005; 50:2597–616. [PubMed: 15901957]
42. Niedre MJ, Secord AJ, Patterson MS, Wilson BC. In vitro tests of the validity of singlet oxygen luminescence measurements as a dose metric in photodynamic therapy. Cancer research. 2003; 63:7986–94. [PubMed: 14633731]
43. Weishaupt KR, Gomer CJ, Dougherty TJ. Identification of singlet oxygen as the cytotoxic agent in photoinactivation of a murine tumor. Cancer research. 1976; 36:2326–9. [PubMed: 1277137]

44. Georgakoudi I, Foster TH. Singlet oxygen- versus nonsinglet oxygen-mediated mechanisms of sensitizer photobleaching and their effects on photodynamic dosimetry. Photochemistry and photobiology. 1998; 67:612–25. [PubMed: 9648527]
45. Georgakoudi I, Nichols M, Foster T. The mechanism of Photofrin photobleaching and its consequences for photodynamic dosimetry. Photochemistry and photobiology. 1997; 65:135–144. [PubMed: 9066293]
46. Aveline B, Redmond R. Can cellular phototoxicity be accurately predicted on the basis of sensitizer photophysics? Photochemistry and photobiology. 1999; 69:306–316. [PubMed: 10089822]
47. Potter WR, Mang TS, Dougherty TJ. The theory of photodynamic therapy dosimetry: consequences of photo-destruction of sensitizer. Photochemistry and photobiology. 1987; 46:97–101. [PubMed: 2956621]
48. Fingar VH, Potter WR, Henderson BW. Drug and light dose dependence of photodynamic therapy: a study of tumor cell clonogenicity and histologic changes. Photochemistry and photobiology. 1987; 45:643–50. [PubMed: 2955431]
49. Betz CS, Rauschning W, Stranadko EP, Riabov MV, Albrecht V, Nifantiev NE, Hopper C. Optimization of treatment parameters for Foscan®-PDT of basal cell carcinomas. Lasers in surgery and medicine. 2008; 40:300–311. [PubMed: 18563776]
50. Mathews M, Angell-Petersen E, Sanchez R, Sun CH, Vo V, Hirschberg H, Madsen S. The effects of ultra low fluence rate single and repetitive photodynamic therapy on glioma spheroids. Lasers in surgery and medicine. 2009; 41:578–662. [PubMed: 19731298]
51. Gibson SL, VanDerMeid KR, Murant RS, Raubertas RF, Hilf R. Effects of various photoradiation regimens on the antitumor efficacy of photodynamic therapy for R3230AC mammary carcinomas. Cancer Res. 1990; 50:7236–41. [PubMed: 2171760]
52. Foster TH, Murant RS, Bryant RG, Knox RS, Gibson SL, Hilf R. Oxygen consumption and diffusion effects in photodynamic therapy. Radiat Res. 1991; 126:296–303. [PubMed: 2034787]
53. Celli JP, Rizvi I, Evans CL, Abu-Yousif AO, Hasan T. Quantitative imaging reveals heterogeneous growth dynamics and treatment-dependent residual tumor distributions in a three-dimensional ovarian cancer model. Journal of Biomedical Optics. 2010; 15:051603–10. [PubMed: 21054077]
54. Rizvi I, Celli JP, Evans CL, Abu-Yousif AO, Muzikansky A, Pogue BW, Finkelstein D, Hasan T. Synergistic enhancement of carboplatin efficacy with photodynamic therapy in a three-dimensional model for micrometastatic ovarian cancer. Cancer Res. 2010; 70:9319–28. [PubMed: 21062986]
55. Cho KR, Shih Ie M. Ovarian cancer. Annu Rev Pathol. 2009; 4:287–313. [PubMed: 18842102]
56. Bast RC Jr, Hennessy B, Mills GB. The biology of ovarian cancer: new opportunities for translation. Nat Rev Cancer. 2009; 9:415–28. [PubMed: 19461667]
57. Siegel R, Naishadham D, Jemal A. Cancer statistics, 2012. CA: a cancer journal for clinicians. 2012; 62:10–29. [PubMed: 22237781]
58. Evans SM, Judy KD, Dunphy I, Jenkins WT, Hwang WT, Nelson PT, Lustig RA, Jenkins K, Magarelli DP, Hahn SM, Collins RA, Grady MS, Koch CJ. Hypoxia is important in the biology and aggression of human glial brain tumors. Clin Cancer Res. 2004; 10:8177–84. [PubMed: 15623592]
59. Evans SM, Judy KD, Dunphy I, Jenkins WT, Nelson PT, Collins R, Wileyto EP, Jenkins K, Hahn SM, Stevens CW, Judkins AR, Phillips P, Geoerger B, Koch CJ. Comparative measurements of hypoxia in human brain tumors using needle electrodes and EF5 binding. Cancer Res. 2004; 64:1886–92. [PubMed: 14996753]
60. Bogaards A, Varma A, Zhang K, Zach D, Bisland SK, Moriyama EH, Lilge L, Muller PJ, Wilson BC. Fluorescence image-guided brain tumour resection with adjuvant metronomic photodynamic therapy: pre-clinical model and technology development. Photochem Photobiol Sci. 2005; 4:438–42. [PubMed: 15875077]
61. Stepp H, Beck T, Pongratz T, Meinel T, Kreth FW, Tonn JC, Stummer W. ALA and malignant glioma: fluorescence-guided resection and photodynamic treatment. Journal of Environmental Pathology, Toxicology & Oncology. 2007; 26:157–64.

62. Beck TJ, Kreth FW, Beyer W, Mehrkens JH, Obermeier A, Stepp H, Stummer W, Baumgartner R. Interstitial photodynamic therapy of nonresectable malignant glioma recurrences using 5-aminolevulinic acid induced protoporphyrin IX. Lasers Surg Med. 2007; 39:386–93. [PubMed: 17565715]
63. Olzowy B, Hundt CS, Stocker S, Bise K, Reulen HJ, Stummer W. Photoirradiation therapy of experimental malignant glioma with 5-aminolevulinic acid. J Neurosurg. 2002; 97:970–6. [PubMed: 12405389]
64. Biel MA. Photodynamic therapy and the treatment of head and neck neoplasia. Laryngoscope. 1998; 108:1259–68. [PubMed: 9738739]
65. de Bree R, Leemans CR. Recent advances in surgery for head and neck cancer. Curr Opin Oncol.
66. Rigual NR, Thankappan K, Cooper M, Sullivan MA, Dougherty T, Popat SR, Loree TR, Biel MA, Henderson B. Photodynamic therapy for head and neck dysplasia and cancer. Arch Otolaryngol Head Neck Surg. 2009; 135:784–8. [PubMed: 19687399]
67. Zhu TC, Finlay JC, Hahn SM. Determination of the distribution of light, optical properties, drug concentration, and tissue oxygenation in-vivo in human prostate during motexafin lutetium-mediated photodynamic therapy. J Photochem Photobiol B. 2005; 79:231–41. [PubMed: 15896650]
68. ClinicalTrials.gov. Sequential Whole Bladder Photodynamic Therapy (WBPDT) in the Management of Superficial Bladder Cancer. 2010. Available at: http://clinicaltrials.gov/ct2/show/NCT00322699?cond=bladder+cancer&intr=photodynamic+therapy&rank=1
69. Chapman MH, Pereira SP. Cholangiocarcinoma: improving biliary drainage with PDT. Photodiagnosis Photodyn Ther. 2009; 6:82–3. [PubMed: 19683206]
70. Pereira, SP. Photodynamic therapy for pancreatic and biliary tract carcinoma; SPIE, Proceedings of the Optical Methods for Tumor Treatment and Detection: Mechanisms and Techniques in Photodynamic Therapy XVIII; San Jose, CA, USA. 2009. p. 71640J-10
71. Sandanayake, NS.; Huggett, MT.; Bown, SG.; Pogue, BW.; Hasan, T.; Pereira, SP. PDT for locally advanced pancreatic cancer: early clinical results. SPIE, Proceedings of the Optical Methods for Tumor Treatment and Detection: Mechanisms and Techniques in Photodynamic Therapy XIX; San Francisco, California, USA. 2010. p. 75510L-8
72. Bown SG, Rogowska AZ, Whitelaw DE, Lees WR, Lovat LB, Ripley P, Jones L, Wyld P, Gillams A, Hatfield AWR. Photodynamic therapy for cancer of the pancreas. Gut. 2002; 50:549–557. [PubMed: 11889078]
73. Ayaru L, Bown SG, Pereira SP. Photodynamic therapy for pancreatic and biliary tract carcinoma. Int J Gastrointest Cancer. 2005; 35:1–13. [PubMed: 15722569]
74. Kessel D, Oleinick NL. Initiation of autophagy by photodynamic therapy. Methods Enzymol. 2009; 453:1–16. [PubMed: 19216899]
75. Oleinick N, Morris R, Belichenko I. The role of apoptosis in response to photodynamic therapy: what, where, why, and how. Photochemical & Photobiological Sciences. 2002; 1:1–21. [PubMed: 12659143]
76. Buytaert E, Dewaele M, Agostinis P. Molecular effectors of multiple cell death pathways initiated by photodynamic therapy. BBA-Reviews on Cancer. 2007; 1776:86–107. [PubMed: 17693025]
77. Kessel D, Luo Y, Deng Y, Chang CK. The role of subcellular localization in initiation of apoptosis by photodynamic therapy. Photochemistry and photobiology. 1997; 65:422–6. [PubMed: 9077123]
78. Kessel D, Luo Y. Mitochondrial photodamage and PDT-induced apoptosis. Journal of photochemistry and photobiology B, Biology. 1998; 42:89–95.
79. Andrzejak M, Price M, Kessel DH. Apoptotic and autophagic responses to photodynamic therapy in 1c1c7 murine hepatoma cells. Autophagy. 2011; 7:979–84. [PubMed: 21555918]
80. Casas A, Di Venosa G, Hasan T, Al B. Mechanisms of resistance to photodynamic therapy. Current medicinal chemistry. 2011; 18:2486–515. [PubMed: 21568910]
81. Verma S, Watt GM, Mai Z, Hasan T. Strategies for enhanced photodynamic therapy effects. Photochem Photobiol. 2007; 83:996–1005. [PubMed: 17880492]
82. Solban N, Rizvi I, Hasan T. Targeted photodynamic therapy. Lasers Surg Med. 2006; 38:522–31. [PubMed: 16671102]

83. Gomer C, Ferrario A, Luna M, Rucker N, Wong S. Photodynamic therapy: combined modality approaches targeting the tumor microenvironment. Lasers in Surgery and Medicine. 2006; 38:516–521. [PubMed: 16607618]
84. Ferrario A, Gomer CJ. Targeting the tumor microenvironment using photodynamic therapy combined with inhibitors of cyclooxygenase-2 or vascular endothelial growth factor. Methods Mol Biol. 2010; 635:121–32. [PubMed: 20552344]
85. Abu-Yousif AO, Moor AC, Zheng X, Savellano MD, Yu W, Selbo PK, Hasan T. Epidermal growth factor receptor-targeted photosensitizer selectively inhibits EGFR signaling and induces targeted phototoxicity in ovarian cancer cells. Cancer letters. 2012; 321:120–7. [PubMed: 22266098]
86. Peng TI, Chang CJ, Guo MJ, Wang YH, Yu JS, Wu HY, Jou MJ. Mitochondrion-targeted photosensitizer enhances the photodynamic effect-induced mitochondrial dysfunction and apoptosis. Annals of the New York Academy of Sciences. 2005; 1042:419–28. [PubMed: 15965088]
87. Granville DJ, Levy JG, Hunt DW. Photodynamic treatment with benzoporphyrin derivative monoacid ring A produces protein tyrosine phosphorylation events and DNA fragmentation in murine P815 cells. Photochem Photobiol. 1998; 67:358–62. [PubMed: 9523536]
88. Belzacq AS, Jacotot E, Vieira HL, Mistro D, Granville DJ, Xie Z, Reed JC, Kroemer G, Brenner C. Apoptosis induction by the photosensitizer verteporfin: identification of mitochondrial adenine nucleotide translocator as a critical target. Cancer Res. 2001; 61:1260–4. [PubMed: 11245415]
89. Celli JP, Solban N, Liang A, Pereira SP, Hasan T. Verteporfin-based photodynamic therapy overcomes gemcitabine insensitivity in a panel of pancreatic cancer cell lines. Lasers in surgery and medicine. 2011; 43:565–74. [PubMed: 22057484]
90. Granville DJ, Levy JG, Hunt DW. Photodynamic therapy induces caspase-3 activation in HL-60 cells. Cell Death Differ. 1997; 4:623–8. [PubMed: 14555976]
91. Granville DJ, Carthy CM, Hunt DW, McManus BM. Apoptosis: molecular aspects of cell death and disease. Lab Invest. 1998; 78:893–913. [PubMed: 9714178]
92. Granville DJ, Carthy CM, Jiang H, Shore GC, McManus BM, Hunt DW. Rapid cytochrome c release, activation of caspases 3, 6, 7 and 8 followed by Bap31 cleavage in HeLa cells treated with photodynamic therapy. FEBS Lett. 1998; 437:5–10. [PubMed: 9804161]
93. Granville DJ, Hunt DW. Porphyrin-mediated photosensitization - taking the apoptosis fast lane. Curr Opin Drug Discov Devel. 2000; 3:232–43.
94. Schmidt-Erfurth U, Hasan T. Mechanisms of Action of Photodynamic Therapy with Verteporfin for the Treatment of Age-Related Macular Degeneration. Surv Ophthalmol. 2000; 45:195–214. [PubMed: 11094244]
95. Duska LR, Hamblin MR, Miller JL, Hasan T. Combination photoimmunotherapy and cisplatin: effects on human ovarian cancer ex vivo. J Natl Cancer Inst. 1999; 91:1557–63. [PubMed: 10491432]
96. del Carmen MG, Rizvi I, Chang Y, Moor AC, Oliva E, Sherwood M, Pogue B, Hasan T. Synergism of epidermal growth factor receptor-targeted immunotherapy with photodynamic treatment of ovarian cancer in vivo. J Natl Cancer Inst. 2005; 97:1516–24. [PubMed: 16234565]
97. Wilson BC, Patterson MS, Lilge L. Implicit and explicit dosimetry in photodynamic therapy: a New paradigm. Lasers in medical science. 1997; 12:182–99. [PubMed: 20803326]
98. Wilson, BBPMSFSTMJD.; Douglas, MDA. The optical absorption and scattering properties of tissues in the visible and near-infrare wavelength range. In: , editor. Light in Biology and medicine. Vol. 1. 1988. 45 p.
99. Dysart JS, Singh G, Patterson MS. Calculation of singlet oxygen dose from photosensitizer fluorescence and photobleaching during mTHPC photodynamic therapy of MLL cells. Photochemistry and photobiology. 2005; 81:196–205. [PubMed: 15469385]
100. Wilson, BC. Photodynamic therapy: light delivery and dosage for second-generation photosensitizers. In: , editor. Photosensitizing compounds: Their chemistry, biology and clinical use. Vol. 146. 1989. p. 60-77.CIBA Found Symp
101. Whitacre CM, Satoh TH, Xue L, Gordon NH, Oleinick NL. Photodynamic therapy of human breast cancer xenografts lacking caspase-3. Cancer letters. 2002; 179:43–9. [PubMed: 11880181]

102. Luo Y, Chang CK, Kessel D. Rapid initiation of apoptosis by photodynamic therapy. Photochemistry and photobiology. 1996; 63:528–34. [PubMed: 8934765]

103. Sheng C, Jack Hoopes P, Hasan T, Pogue B. Photobleaching-based dosimetry predicts deposited dose in ALA-PpIX PDT of rodent esophagus. Photochemistry and photobiology. 2007; 83:738–748. [PubMed: 17576383]

104. Glidden MD, Celli JP, Massodi I, Rizvi I, Pogue BW, Hasan T. Image-Based Quantification of Benzoporphyrin Derivative Uptake, Localization, and Photobleaching in 3D Tumor Models, for Optimization of PDT Parameters. Theranostics. 2012; 2:827–39. [PubMed: 23082096]

105. Evans CL, Abu-Yousif AO, Park YJ, Klein OJ, Celli JP, Rizvi I, Zheng X, Hasan T. Killing hypoxic cell populations in a 3D tumor model with EtNBS-PDT. PLoS One. 2011; 6:e23434. [PubMed: 21876751]

106. Celli J, Rizvi I, Evans C, Abu Yousif A, Hasan T. Quantitative imaging reveals heterogeneous growth dynamics and treatment-dependent residual tumor distributions in a three-dimensional ovarian cancer model. Journal of biomedical optics. 2010; 15:051603. [PubMed: 21054077]

107. Rizvi I, Celli JP, Evans CL, Abu-Yousif AO, Muzikansky A, Pogue BW, Finkelstein D, Hasan T. Synergistic enhancement of carboplatin efficacy with photodynamic therapy in a three-dimensional model for micrometastatic ovarian cancer. Cancer research. 2010; 70:9319–9328. [PubMed: 21062986]

108. Celli J, Rizvi I, Blanden A, Abu-Yousif AO, Spring B, Hasan T. Biologically-relevant 3D tumor arrays: Imaging-based methods for quantification of reproducible growth and analysis of treatment response. Proc SPIE. 2011:7886–7.

109. Celli JP, Rizvi I, Evans CL, Abu-Yousif AO, Hasan T. 3D ovarian cancer models: imaging and therapeutic combinations. Proc SPIE. 2010:7551.

110. Celli J, Rizvi I, Blanden A, Evans C, Abu-Yousif A, Spring B, Muzikansky A, Pogue B, Finkelstein D, Hasan T. Imaging Enabled Platforms for Development of Therapeutics. Proc SPIE. 2011:7910–1.

111. Zhong W, Celli JP, Rizvi I, Mai Z, Spring BQ, Yun SH, Hasan T. In vivo high-resolution fluorescence microendoscopy for ovarian cancer detection and treatment monitoring. British journal of cancer. 2009; 101:2015–22. [PubMed: 19920823]

112. Ascencio M, Collinet P, Farine MO, Mordon S. Protoporphyrin IX fluorescence photobleaching is a useful tool to predict the response of rat ovarian cancer following hexaminolevulinate photodynamic therapy. Lasers Surg Med. 2008; 40:332–41. [PubMed: 18563777]

113. Ascencio M, Estevez JP, Delemer M, Farine MO, Collinet P, Mordon S. Comparison of continuous and fractionated illumination during hexaminolaevulinate-photodynamic therapy. Photodiagnosis Photodyn Ther. 2008; 5:210–6. [PubMed: 19356657]

114. Estevez JP, Ascencio M, Colin P, Farine MO, Collinet P, Mordon S. Continuous or fractionated photodynamic therapy? Comparison of three PDT schemes for ovarian peritoneal micrometastasis treatment in a rat model. Photodiagnosis Photodyn Ther. 2010; 7:251–7. [PubMed: 21112548]

115. Guyon L, Ascencio M, Collinet P, Mordon S. Photodiagnosis and photodynamic therapy of peritoneal metastasis of ovarian cancer. Photodiagnosis and photodynamic therapy. 2012; 9:16–47. [PubMed: 22369725]

116. Molpus KL, Hamblin MR, Rizvi I, Hasan T. Intraperitoneal Photoimmunotherapy of Ovarian Carcinoma Xenografts in Nude Mice Using Charged Photoimmunoconjugates. Gynecol Oncol. 2000; 76:397–404. [PubMed: 10684717]

117. Molpus KL, Kato D, Hamblin MR, Lilge L, Bamberg M, Hasan T. Intraperitoneal photodynamic therapy of human epithelial ovarian carcinomatosis in a xenograft murine model. Cancer Res. 1996; 56:1075–82. [PubMed: 8640764]

118. Zuluaga MF, Lange N. Combination of photodynamic therapy with anti-cancer agents. Curr Med Chem. 2008; 15:1655–73. [PubMed: 18673216]

119. Cengel KA, Glatstein E, Hahn SM. Intraperitoneal photodynamic therapy. Cancer Treat Res. 2007; 134:493–514. [PubMed: 17633077]

120. Menon C, Kutney SN, Lehr SC, Hendren SK, Busch TM, Hahn SM, Fraker DL. Vascularity and uptake of photosensitizer in small human tumor nodules: implications for intraperitoneal photodynamic therapy. Clin Cancer Res. 2001; 7:3904–11. [PubMed: 11751481]

121. Dysart JS, Patterson MS, Farrell TJ, Singh G. Relationship between mTHPC fluorescence photobleaching and cell viability during in vitro photodynamic treatment of DP16 cells. Photochemistry and photobiology. 2002; 75:289–95. [PubMed: 11950095]

122. McIlroy BWM, Dysart TS, Wilson JS, BC. The effects of oxygenation and photosensitizer substrate binding on the use of fluorescence photobleaching as a dose metric for photodynamic therapy. Vibrational Spectroscopy. 2002; 28:25–35.

123. Kessel D, Arroyo AS. Apoptotic and autophagic responses to Bcl-2 inhibition and photodamage. Photochem Photobiol Sci. 2007; 6:1290–5. [PubMed: 18046484]

124. Xue L, Chiu S, Oleinick N. Photochemical destruction of the Bcl-2 oncoprotein during photodynamic therapy with the phthalocyanine photosensitizer Pc 4. Oncogene. 2001; 20:3420–3427. [PubMed: 11423992]

125. Winter W, Maxwell G, Tian C, Sundborg M, Rose G, Rose P, Rubin S, Muggia F, McGuire W. G. Gynecologic Oncology . Tumor residual after surgical cytoreduction in prediction of clinical outcome in stage IV epithelial ovarian cancer: a Gynecologic Oncology Group Study. Journal of clinical oncology: official journal of the American Society of Clinical Oncology. 2008; 26:83–92. [PubMed: 18025437]

126. Hoskins WJ, McGuire WP, Brady MF, Homesley HD, Creasman WT, Berman M, Ball H, Berek JS. The effect of diameter of largest residual disease on survival after primary cytoreductive surgery in patients with suboptimal residual epithelial ovarian carcinoma. American journal of obstetrics and gynecology. 1994; 170:974–9. discussion 979–80. [PubMed: 8166218]

127. Eisenhauer E, Abu-Rustum N, Sonoda Y, Aghajanian C, Barakat R, Chi D. The effect of maximal surgical cytoreduction on sensitivity to platinum-taxane chemotherapy and subsequent survival in patients with advanced ovarian cancer. Gynecologic oncology. 2008; 108:276–357. [PubMed: 18063020]

128. Eisenhauer EL, Abu-Rustum NR, Sonoda Y, Aghajanian C, Barakat RR, Chi DS. The effect of maximal surgical cytoreduction on sensitivity to platinum-taxane chemotherapy and subsequent survival in patients with advanced ovarian cancer. Gynecol Oncol. 2008; 108:276–81. [PubMed: 18063020]

129. Chi DS, Eisenhauer EL, Zivanovic O, Sonoda Y, Abu-Rustum NR, Levine DA, Guile MW, Bristow RE, Aghajanian C, Barakat RR. Improved progression-free and overall survival in advanced ovarian cancer as a result of a change in surgical paradigm. Gynecol Oncol. 2009; 114:26–31. [PubMed: 19395008]

130. Lee S, Isabelle ME, Gabally-Kinney KL, Pogue BW, Davis SJ. Dual-channel imaging system for singlet oxygen and photosensitizer for PDT. Biomedical optics express. 2011; 2:1233–42. [PubMed: 21559134]

131. Laubach HJ, Chang SK, Lee S, Rizvi I, Zurakowski D, Davis SJ, Taylor CR, Hasan T. In-vivo singlet oxygen dosimetry of clinical 5-aminolevulinic acid photodynamic therapy. Journal of biomedical optics. 2008; 13:050504. [PubMed: 19021376]

132. Georgakoudi I. Singlet oxygen- versus nonsinglet oxygen-mediated mechanisms of sensitizer photobleaching and their effects on photodynamic dosimetry. Photochemistry & Photobiology. 1998; 67:612–25. [PubMed: 9648527]

133. Aveline BM, Redmond RW. Can cellular phototoxicity be accurately predicted on the basis of sensitizer photophysics? Photochem Photobiol. 1999; 69:306–16. [PubMed: 10089822]

134. Aveline BM, Sattler RM, Redmond RW. Environmental effects on cellular photosensitization: correlation of phototoxicity mechanism with transient absorption spectroscopy measurements. Photochemistry and photobiology. 1998; 68:51–62. [PubMed: 9679451]

135. Baran T, Foster T. Fluence rate-dependent photobleaching of intratumorally administered Pc 4 does not predict tumor growth delay. Photochemistry and photobiology. 2012; 88:1273–1279. [PubMed: 22582826]

136. Xue LY, Chiu SM, Oleinick NL. Photodynamic therapy-induced death of MCF-7 human breast cancer cells: a role for caspase-3 in the late steps of apoptosis but not for the critical lethal event. Exp Cell Res. 2001; 263:145–55. [PubMed: 11161713]

137. Porter AG, Janicke RU. Emerging roles of caspase-3 in apoptosis. Cell Death Differ. 1999; 6:99–104. [PubMed: 10200555]

138. Kessel D, Reiners JJ Jr. Initiation of apoptosis and autophagy by the Bcl-2 antagonist HA14-1. Cancer Lett. 2007; 249:294–9. [PubMed: 17055152]

139. Donohue E, Tovey A, Vogl AW, Arns S, Sternberg E, Young RN, Roberge M. Inhibition of autophagosome formation by the benzoporphyrin derivative verteporfin. J Biol Chem. 2011; 286:7290–300. [PubMed: 21193398]

140. Osaki T, Takagi S, Hoshino Y, Okumura M, Fujinaga T. Intracellular localization and concentration as well as photodynamic effects of benzoporphyrin derivative monoacid ring A in four types of rodent tumor cells. Cancer Lett. 2006; 243:281–92. [PubMed: 16412570]

141. Rizvi I, Dinh TA, Yu W, Chang Y, Sherwood ME, Hasan T. Photoimmunotherapy and Irradiance Modulation Reduce Chemotherapy Cycles and Toxicity in a Murine Model for Ovarian Carcinomatosis: Perspective and Results. Israel Journal of Chemistry. 2012; 52:776–787. [PubMed: 23626376]

142. Major AL, Rose GS, Svaasand LO, Ludicke F, Campana A, van Gemert MJ. Intraperitoneal photodynamic therapy in the Fischer 344 rat using 5-aminolevulinic acid and violet laser light: a toxicity study. J Photochem Photobiol B. 2002; 66:107–14. [PubMed: 11897510]

143. Haber D, Gray N, Baselga J. The evolving war on cancer. Cell. 2011; 145:19–24. [PubMed: 21458664]

144. Bigelow CE, Mitra S, Knuechel R, Foster TH. ALA- and ALA-hexylester-induced protoporphyrin IX fluorescence and distribution in multicell tumour spheroids. Br J Cancer. 2001; 85:727–34. [PubMed: 11531259]

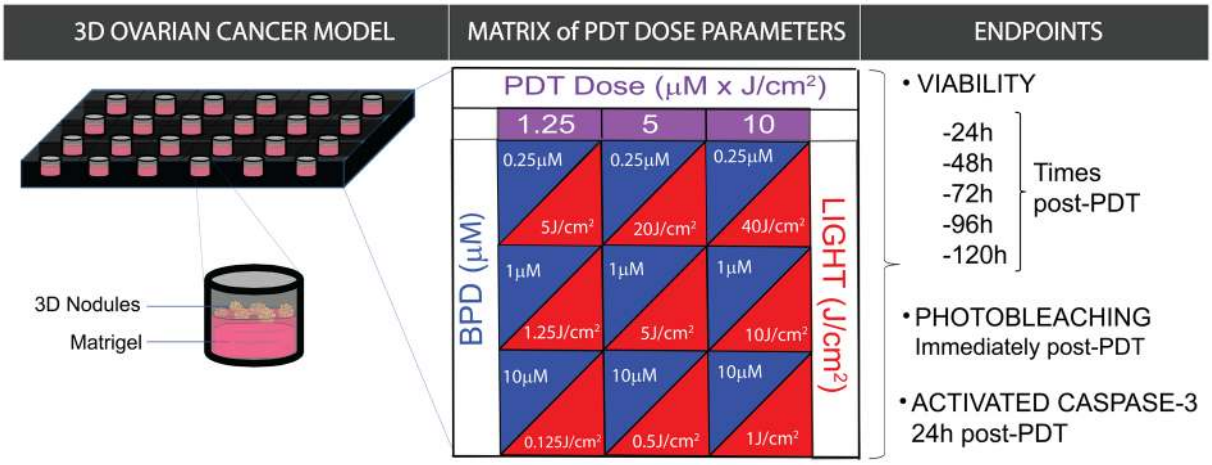

FIGURE 1. Experimental schema

A three-dimensional (3D) model for ovarian cancer (OvCa) was used to determine the effects of modulating photodynamic therapy (PDT) parameters on tumoricidal durability (left). A matrix of benzoporphyrin derivative (BPD) concentrations (0.25 μM, 1 μM, or 10 μM) (blue) and fluences (0.125 J/cm^2 – 40 J/cm^2 @ 150 mW/cm^2) (red) was established to differentially construct three fixed PDT doses (1.25, 5, or 10 μM × J/cm^2) (purple) (middle). Viability was evaluated every 24 hours for 5 days post-PDT as the key therapeutic endpoint. Photobleaching (immediately post-PDT) and activated caspase-3 levels (24 hours post-PDT) were assessed as implicit metrics of therapeutic efficacy (right).

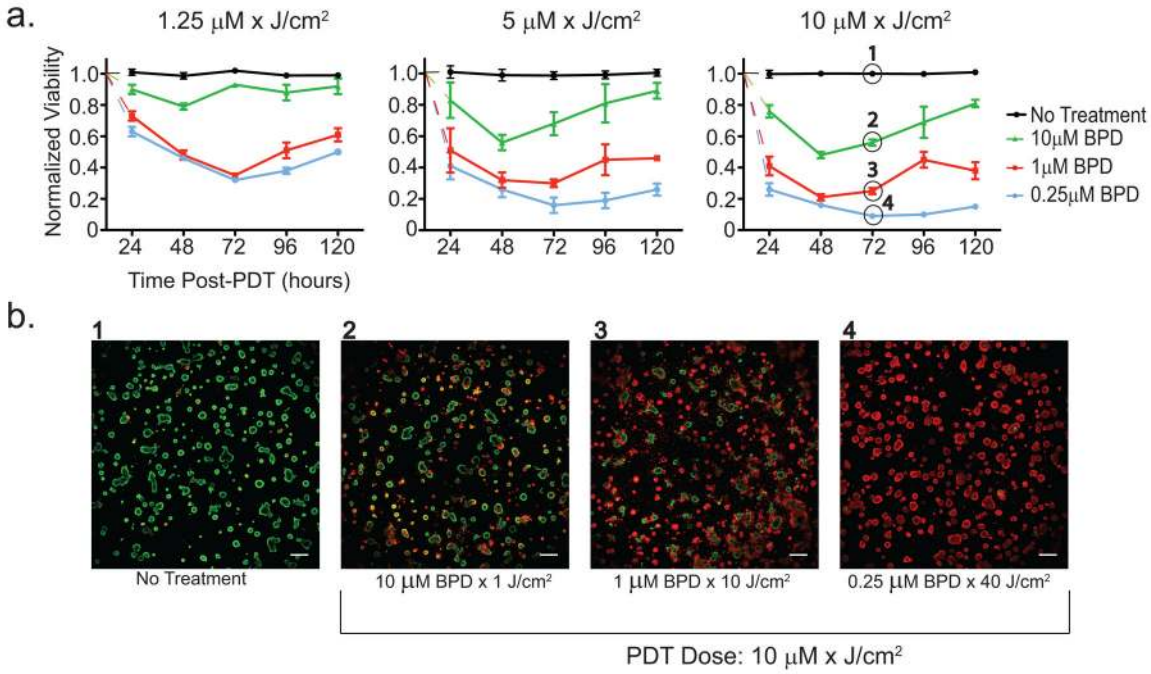

FIGURE 2. The photosensitizer-light parameters used to construct a given PDT dose significantly impact tumoricidal durability

(a.) Normalized viabilities of 3D ovarian micronodules evaluated every 24 hours for 5 days following PDT with 1.25, 5 or 10 μm × J/cm^2. Relative to controls (black), PDT with 0.25 μM BPD (blue) produced the most significant and sustained reduction in normalized viability for all doses, compared to 1 μM (red) or 10 μM BPD-PDT (green) (one-way ANOVA, N ≥6 for 24–96 hours post-PDT, N=4 for 120 hours post-PDT; error bars indicate s.e.m.). (b.) Representative LIVE/DEAD images used to quantify the normalized viabilities plotted in 2A. Images show typical fluorescence patterns from live cells (green, calcein) and dead cells (red, ethidium homodimer-1) for no treatment (1) or following PDT with 10 μm × J/cm^2 (2–4) using 10 μm BPD × 1 J/cm^2 light (2), 1 μm BPD × 10 J/cm^2 (3), or 0.25 μm BPD × 40 J/cm^2 (4), which correspond to the values circled in 2a at 72 hours.

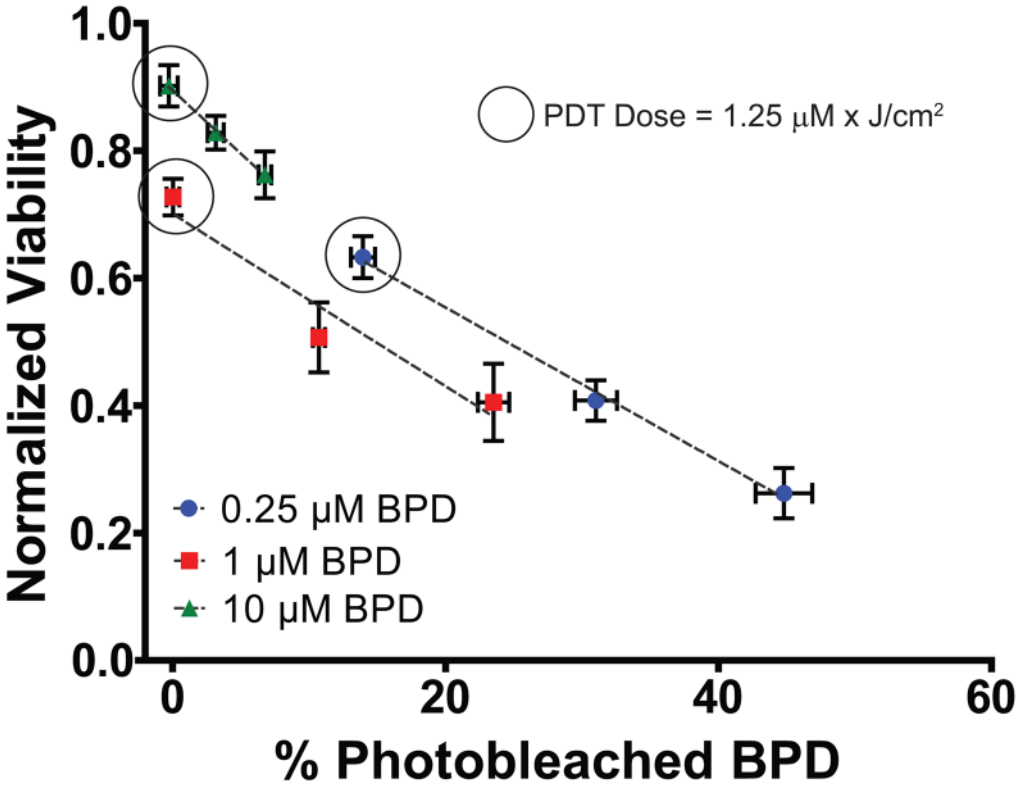

FIGURE 3. Normalized viability correlates linearly with percent photobleaching within BPD concentrations

A correlation between percent photobleaching (evaluated immediately post-PDT) and normalized viability (assessed 24 hours post-PDT) was observed within each concentration of BPD: (i) 0.25 μM (blue) (r^2=0.9962); (ii) 1 μM (red) (r^2=0.9332); and (iii) 10 μM (green) (r^2=0.9982) (Data were fit via linear regression, N ≥4 wells for each data point, error bars indicate s.e.m.). There was a non-linear decrease in viability with percent photobleaching within each PDT dose (for example, 1.25 μM*J/cm^2 denoted with circles).

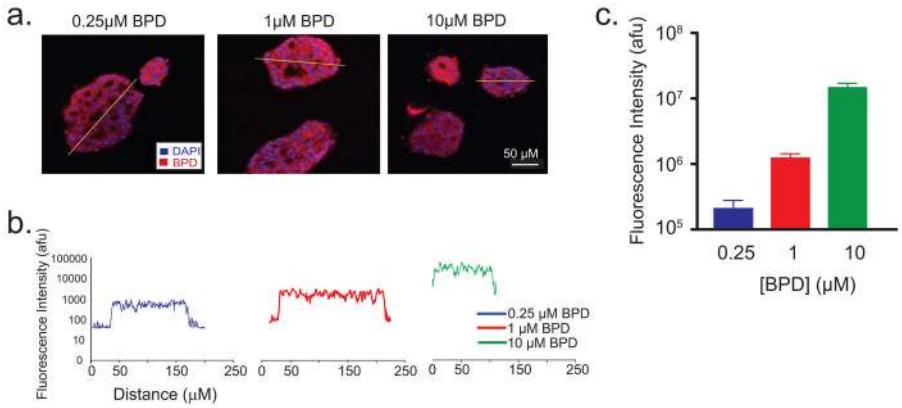

FIGURE 4. BPD fluorescence from 3D ovarian micronodule sections indicates distribution and concentration-dependent BPD uptake

(a.) Fluorescence images (red, BPD; blue, DAPI) from representative cryosections of 10 day-old 3D micronodules and corresponding fluorescence incubated with and (b.) fluorescence intensity profiles show distribution of BPD throughout tumor micronodules for all concentrations (0.25 μM (blue), 1 μM (red), and 10 μM (green)). (c.) Mean fluorescence intensity for 0.25 μM BPD (blue, $2.1 \times 10^5 \pm 7.0 \times 10^4$) was significantly lower than 1 μM BPD (red, $1.2 \times 10^6 \pm 2.1 \times 10^5$) and 10 μM BPD (green, $1.5 \times 10^7 \pm 2.5 \times 10^6$) (one-way ANOVA, n=5 3D nodules for each concentration, error bars indicate s.e.m.).

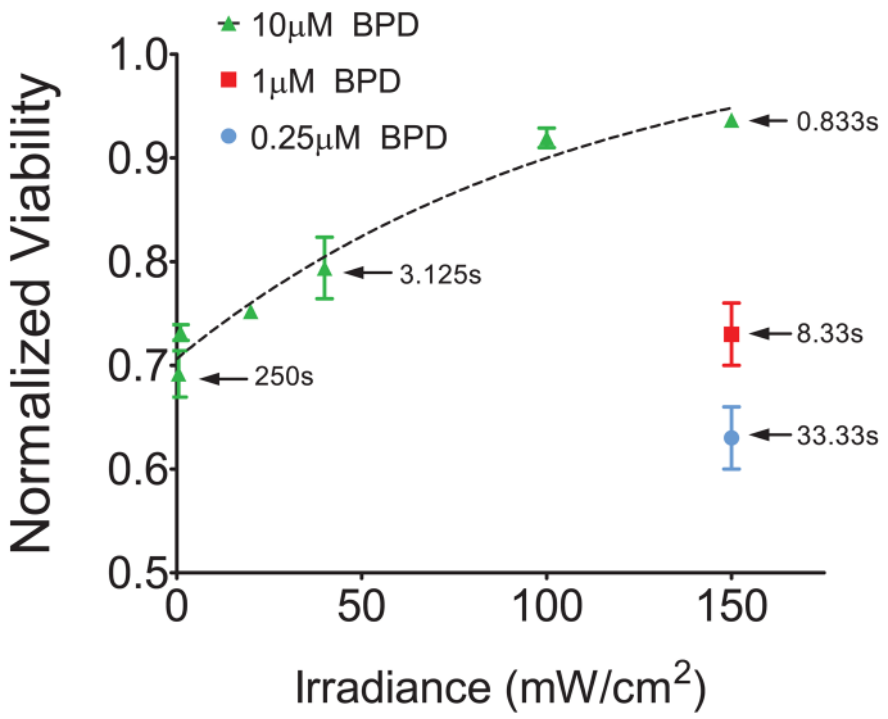

FIGURE 5. Decreasing irradiance improves the cytotoxic efficacy of 10μM BPD-PDT

Normalized viability is significantly higher at an irradiance of 150 mW/cm^2 than lower irradiances 24 hours following treatment with 10 μM BPD-PDT (green) at a fixed dose of 1.25 μM × J/cm^2 (p<0.05, one-way ANOVA, N=6). Decreasing the irradiance to 0.5 mW/cm^2, while keeping the PDT dose constant, reduces normalized viability of nodules treated with 10 μM BPD-PDT to levels that were not significantly different from 0.25 μM BPD-PDT (blue) or 1 μM BPD-PDT (red). Select data points are labeled with the irradiation times required to achieve a constant PDT dose. An asymptotic exponential growth model was used to fit viability and irradiance for nodules treated with 10 μM BPD-PDT (r^2=0.8411).

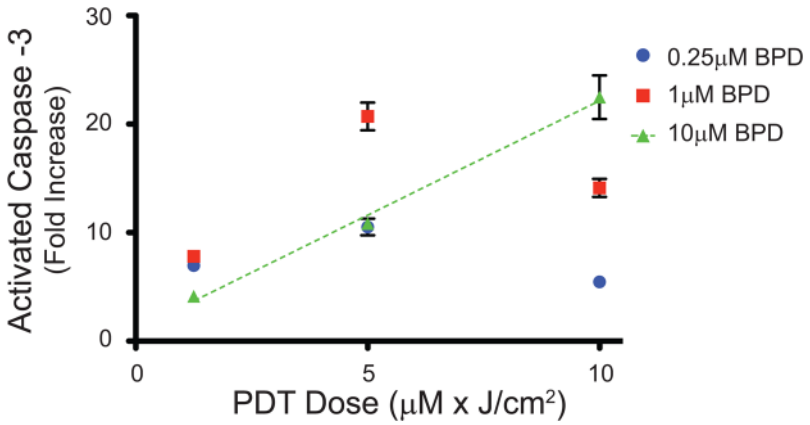

FIGURE 6. Activated Caspase-3 Correlates with PDT dose under limited conditions

Fold increase in activated caspase-3, relative to no treatment controls, is plotted against PDT dose for BPD concentrations of 0.25 μM (blue), 1 μM (red), and 10 μM (green). A significant correlation was observed between activated caspase-3 and PDT dose for 10 μM BPD-PDT ($r^2 = 0.995$, $P<0.05$), but there was no relationship for either 0.25 μM BPD-PDT or 1 μM BPD-PDT.